A bond graph approach to modeling the anuran vocal production system

Nicole M. Kime[a)]
*Department of Biological Sciences, Edgewood College, 1000 Edgewood College Drive,
Madison, Wisconsin 53711*

Michael J. Ryan
*Section of Integrative Biology, University of Texas at Austin, 1 University Station C0990,
Austin, Texas 78712*

Preston S. Wilson
*Department of Mechanical Engineering, University of Texas at Austin, 1 University Station C2200,
Austin, Texas 78712*

Air-driven vocal production systems such as those found in mammals, birds, and anurans (frogs and toads) combine pneumatic and mechanical elements in species-specific ways to produce a diversity of communication signals. This study uses bond graphs to model a generalized anuran vocal production system. Bond graphs allow an incremental approach to modeling dynamic physical systems involving different domains. Anurans provide an example of how signal diversity results from variation in the structure and behavior of vocal system elements. This paper first proposes a bond graph model of the integrated anuran vocal system as a framework for future study. It then presents a simulated submodel of the anuran sound source that produces sustained oscillations in vocal fold displacement and air flow through the larynx. The modeling approach illustrated here should prove of general applicability to other biological sound production systems, and will allow researchers to study the biomechanics of vocal production as well as the functional congruence and evolution of groups of traits within integrated vocal systems.
© 2013 Acoustical Society of America. [http://dx.doi.org/10.1121/1.4802743]

I. INTRODUCTION

Communication is central to social behavior in a wide range of animal taxa, and acoustic communication is the most widely studied of all modalities. Despite the importance and prevalence of acoustic signals, detailed understanding of the biomechanics of sound production has proven elusive in many taxa. This paper reports on one approach to modeling sound production in anurans (frogs and toads) that should prove of general applicability to other biological sound production systems.

Air-driven vocal production systems such as those found in mammals, birds, and anurans combine a few basic types of pneumatic and mechanical elements in species-specific ways to produce an astounding diversity of signals. Such systems can be divided into three major components (Fitch and Hauser, 2003; Fletcher, 1992). The first component is a pair of compressible air volumes (the lungs) that supply flow to the system. The second component is a sound source (the larynx in anurans and mammals, or the syrinx in birds) that contains a mechanical valve that can be induced into sustained oscillations. Air flow from the lungs is converted into pressure variations as it moves through a variable constriction within the sound source. This sound is then passed through the third component, a supra-laryngeal (mammals and anurans) or supra-syringeal (birds) vocal tract. After coupling to the environment, the sound can be perceived as an acoustic signal by a receiver.

Quantitative approaches to modeling vocal production are common in humans and birds (e.g., Elemans *et al.*, 2003; Fletcher, 1988; Story, 2002; Titze, 2000), with a few models in other vertebrate taxa (e.g., Aroyan *et al.*, 2000; de Boer, 2009; Riede *et al.*, 2011). Models that describe individual components of the vocal production system provide valuable insights into the role of specific anatomical parameters in signal production. These insights can be limited, however, when there are significant interactions among components in the system (Fletcher and Thwaites, 1979). Thus, quantitative models that integrate vocal system components can allow for the investigation of signal properties that cannot be predicted from the behavior of any one component in isolation.

One approach to modeling integrated vocal production systems is to use lumped element models in which the mechanical and pneumatic elements of the system are viewed as analogous to the elements of electrical circuits (Fletcher and Thwaites, 1979; Fletcher, 1992). As in electrical circuits (with their inductors, capacitors, and resistors), the goal is to create a network of simplified vocal system elements (masses, springs, and dampers for mechanical oscillators; and volumes, tubes, and apertures in the pneumatic domain). In acoustics, these lumped-element models are valid as long as the acoustic wavelength is much greater than the largest physical dimension of the system.

a)Author to whom correspondence should be addressed. Electronic mail: nkime@edgewood.edu

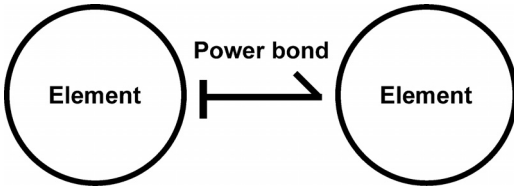FIG. 1. Conceptual design of bond graphs as the transfer of energy between two elements.
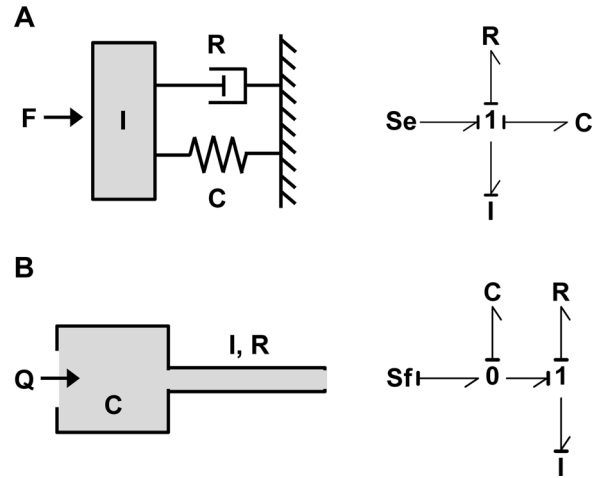

FIG. 2. Schematic and bond graph representations of (A) a simple mass-spring-damper system in the mechanical domain and (B) flow into a fluid capacitance and through a narrow pipe in the pneumatic domain.

This paper reports on a bond graph approach to modeling a generalized anuran vocal production system. Sections II and III provide an introduction to bond graphs and the anuran vocal system. Section IV describes a bond graph model of the generalized anuran vocal system as a framework for modeling vocal production in this taxon. Section V presents results of a bond graph simulation of sustained oscillations in the anuran sound source using biologically relevant system parameters. Section VI suggests how the approach presented here might be further used to model the biomechanics of vocal production and the evolution of integrated vocal systems in anurans and other animals.

II. PRINCIPLES OF BOND GRAPH MODELING FOR ANIMAL VOCAL SYSTEMS

A bond graph approach to lumped element modeling has several advantages for modeling animal vocal systems. First, it uses intuitive graphical representations and an object-oriented paradigm that is easy to understand and communicate (Borutzky, 2010). Second, bond graphs are domain-independent; a set of common elements can be used to describe both pneumatic and mechanical components of the vocal system (Breedveld, 2004; Busch-Vishniac and Paynter, 1989). Third, one can take an incremental approach to modeling integrated vocal systems by investigating individual system components and then connecting submodels to investigate their interactions (Borutzsky, 2009). Finally, systematic methods are available to derive causal bond graph models and then convert them into a set of equations that can be used to simulate the system (e.g., Karnopp *et al.*, 2006). This section provides an introduction to bond graphs for vocal system modeling. The interested reader is directed to the references above for a more complete description of bond graph modeling.

A. Energy and power transfer

Bond graphs are comprised of *elements* connected by *power bonds* through which energy is transferred in an ideal manner, meaning that no energy is lost in the bonds (Fig. 1). The rate at which energy is transferred between elements is expressed as power (Table I). The direction of positive power transfer in a bond graph is denoted by the direction of the *half-arrow* at one end of the power bond (Fig. 1).

Power can be expressed as the product of an effort variable and a flow variable (Table I). In the mechanical domain, power is the product of force and velocity; in the pneumatic domain, power is the product of pressure and volume flow rate. For a given element in a bond graph, if an effort is its input then a flow must be its conjugate output. Likewise, if a flow is the input to a bond graph element then an effort must be its conjugate output. The perpendicular line at one end of each power bond, called the *causal stroke*, denotes the element to which effort is input at each bond (Fig. 1).

B. Bond graph elements

Eight different types of bond graph elements are necessary to model air-driven vocal systems. These elements are described here and illustrated in Fig. 2, which shows two submodels that are commonly used in lumped-element models of vocal production: a mass-spring-damper system in the mechanical domain and air flow into a compressible volume and then through a tube in the pneumatic domain (e.g., Fletcher, 1992). Table II summarizes the elements.

The elements **Se** and **Sf** represent the addition of effort or flow to the system from an outside source. Examples include force pushing against a mass in the mechanical

TABLE I. Energy and power variables for bond graph modeling in the mechanical and pneumatic domains. Symbols and units indicated follow Karnopp *et al.* (2006) and are those used in the remainder of the paper.

	Relationship	Mechanical	Pneumatic
Energy	–	(N-m)	(N-m)
Power	Rate of energy transfer	(N-m/s)	(N-m/s)
Effort	Power = effort * flow	F = Force (N)	P = Pressure (N/m^2 = Pa)
Flow	Power = effort * flow	v = Velocity (m/s)	Q = Volume flow rate (m^3/s)
Momentum	$\int^t \mathrm{effort}(t)dt$	p = Momentum (N-s)	p_p = Pressure momentum (N-s/m^2)
Displacement	$\int^t \mathrm{flow}(t)dt$	X = Displacement (m)	V = Volume (m^3)

TABLE II. Summary of bond graph elements.

Element	Type
Sf	Source (flow)
Se	Source (effort)
C	Storage (flow)
I	Storage (effort)
R, MR	Dissipative (effort or flow)
TF	Energy transformer
0-junction	Connector (distributes flow)
1-junction	Connector (distributes effort)

domain [**Se**, Fig. 2(A)] and the rate at which a volume of air enters a pneumatic system [**Sf**, Fig. 2(B)]. **Se** elements have a required effort-out causality; this is denoted by the causal stroke in Fig. 2(A). Because the output of **Sf** elements are a flow, they have a required effort-in causality.

All **I** elements store effort through an integration process. Examples of **I** elements are masses in the mechanical domain (which store force in their momentum) and fluid in a pipe in the pneumatic domain (which stores pressure in its pressure momentum) (Fig. 2, Table I). **I** elements have a preferred effort-in causality, which means that their conjugate output is velocity in the mechanical domain or volume flow rate in the pneumatic domain. One can also think of **I** elements as kinetic energy storage.

Elements **C** store flow through an integration process. Examples of **C** elements are springs in the mechanical domain (which store velocity in their displacement) and fluid capacitances in the pneumatic domain (which store volume flow rates in their volume) (Fig. 2, Table I). **C** elements have a preferred effort-out causality, meaning that their conjugate output is force in the mechanical domain or pressure in the pneumatic domain. One can also think of **C** elements as potential energy storage.

All **R** elements represent dissipation of energy into a form that is unavailable to do further work in the system. Dampers and friction are examples of **R** elements [Figs. 2(A), 2(B) respectively]. Although energy flow (and thus the half-arrow of a power bond) must always be toward an **R** element, they are indifferent to causality because they can dissipate either effort or flow. In some cases, the resistance value is determined by a variable input signal. An example is an aperture whose opening is modulated by an outside source. These are modeled as **MR** elements, or modulated resistors.

Transformer elements, **TF**, transform energy from one form to another without storage or loss. **TF** elements can transform either effort or flow. They can be used to translate between pneumatic and mechanical domains; an example is the transformation from pneumatic pressure to mechanical force. A dimensionless parameter (n) serves as the transform ratio, so that $effort_{out} = n * effort_{in}$ or $flow_{out} = n * flow_{in}$ and power is conserved across the transformer.

The **0-** and **1-junctions** couple elements together with no storage or loss of energy. At **0-junctions**, flow is distributed among connections such that the sum of flows is zero considering the direction of the half arrow. Effort is constant, and is determined by one and only one of the bonds connected to the junction. They are thus the equivalent of a

parallel connection in an electrical circuit. In Fig. 2(B), the **0-junction** indicates that some of the flow input to the pneumatic system is stored in the fluid capacitance while the remainder exits through the pipe.

At **1-junctions**, effort is distributed among connections such that the sum of efforts is zero considering the direction of the half arrow. Flow is constant, and is determined by one and only one of the bonds connected to the junction. They are thus the equivalent of a serial connection in an electrical circuit. In Fig. 2(A), the **1-junction** indicates that the force input to the mechanical mass-spring-damper system is partitioned among its elements.

C. Model simulation and analysis

Elements are assembled into bond graph models by tracking power flow through the system. Systematic methods are available to derive causal bond graph models both by hand (e.g., Karnopp *et al.*, 2006) and through the use of commercially available software. Another systematic process is then used to convert the bond graph into a set of system equations that can be solved to simulate the system. These equations identify source inputs and initial conditions, and include the constitutive relationships for all of the elements. Constitutive relationships can be linear or nonlinear. Derivation of equations can also be done by hand or using commercially available software.

For example, in Fig. 2(A), the future displacement of the mass could be determined from the derived system equations given knowledge of the system's driving force, the initial displacement and velocity of the mass, and the constitutive relationships for the mass, spring, and damper. Typical linear constitutive relationships for this system relate the velocity of the mass directly to its momentum, the restoring force of the spring to its displacement via a spring constant, and the force dissipated by the damper (dashpot) to the velocity of the system via a damping coefficient.

III. THE ANURAN VOCAL SYSTEM

Anurans provide an excellent example of how variation in the structure and behavior of common vocal system elements results in signal diversity. The advertisement calls of anurans are used to attract females and mediate male-male interactions (Gerhardt and Huber, 2002; Ryan, 2001). They are species-specific and range from simple tonal signals to complex calls containing frequency modulation, harmonics, continuous amplitude modulation, repeating pulses, and/or nonlinear components (Fig. 3).

A schematic of the generalized anuran vocal production system is shown in Fig. 4. The lungs of frogs and toads are simple air sacs (Gans, 1973). When compressed by the contraction of body wall muscles, they serve as a source of air flow to the rest of the vocal system (Fitch and Hauser, 2003; Martin and Gans, 1972). Flow enters the larynx through a pair of bronchial passages; most anurans lack the longer bronchial tubes found in mammals and birds (Duellman and Trueb, 1994).

The anuran laryngeal apparatus is represented in Fig. 4 as two volumes of air (the posterior and anterior laryngeal
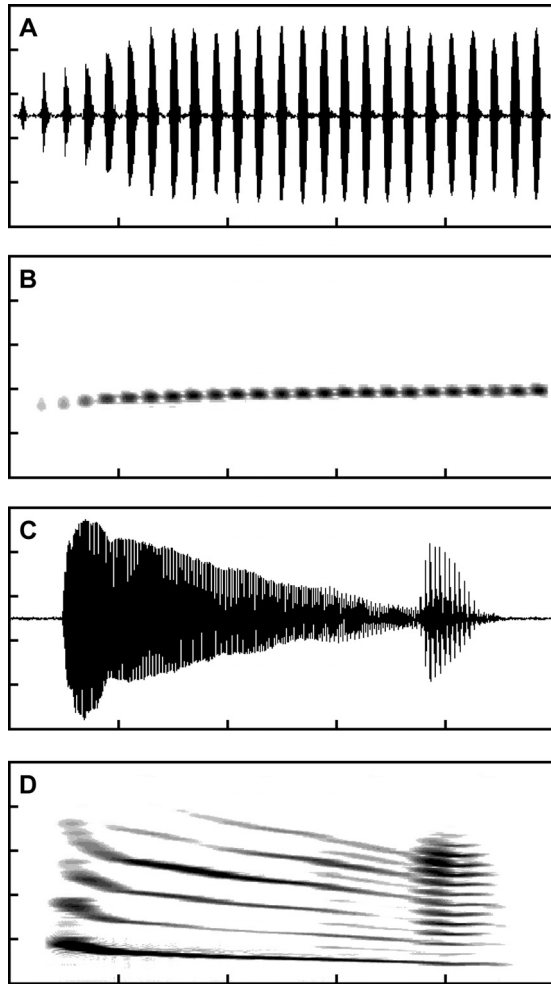
FIG. 3. Examples of two anuran calls. Oscillogram (A) and spectrogram (B) of the pulsed call of the American toad (*Bufo americanus*). Only the first 500 ms of the call is shown. Oscillogram (C) and spectrogram (D) of the amplitude and frequency modulated "whine-chuck" call of the túngara frog (*Physalaemus pustulosus*). Note the subharmonics present near the end of the whine. The chuck is not present in all calls.

chambers) separated by a pair of elastic vocal folds and bounded by a pair of arytenoid cartilages with a ring of cricoid cartilage at their base (Duellman and Trueb, 1994). In an inactive larynx, the arytenoids are closed due to their inherent elasticity. As the anterior margins of the arytenoids open, they pivot inside the rigid cricoid ring. Opening of the
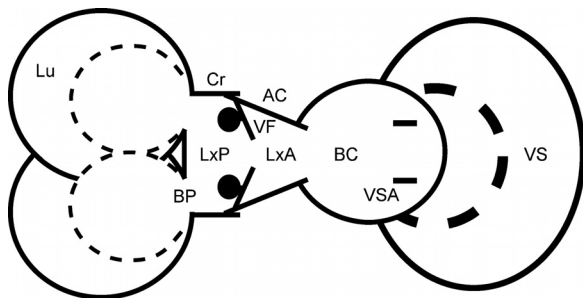

FIG. 4. Vocal system of a generalized anuran. Lu = lungs, BP = bronchial passages, LxP = posterior laryngeal chamber, Cr = cricoid cartilage, VF = vocal folds with fibrous masses, LxA = anterior laryngeal chamber, AC = arytenoid cartilages, BC = buccal cavity, VSA = vocal sac apertures, VS = vocal sac.

arytenoids can occur passively because of an increase in pressure in the posterior laryngeal chamber (Gans, 1973; Martin, 1971). Three pairs of muscles also actively influence the opening and closing of the arytenoids (Duellman and Trueb, 1994). During call production, anuran taxa vary extensively in the relative roles of pressure and muscular control in opening and closing the arytenoid cartilages (Martin, 1971; Schmidt, 1965).

The vocal folds are membranous extensions of the lining of the arytenoids. They attach to both the arytenoid cartilages and the cricoid cartilage: as the arytenoids open the vocal folds are thus stretched and tension increases (Duellman and Trueb, 1994). In some anurans, mass is added to the vocal folds by local thickenings within the folds or pendulous masses suspended from them (Duellman and Trueb, 1994; Martin, 1971; Ryan and Drewes, 1990). These masses may also be responsible for nonlinear signal properties (e.g., Gridi-Papp *et al.*, 2006; Suthers *et al.*, 2006; see Fig. 3). Flow through the anuran larynx thus proceeds from the posterior laryngeal chamber, between the vocal folds, into the anterior laryngeal chamber, and out of the larynx through a vertical aperture between the arytenoid cartilages.

The anuran supra-laryngeal vocal tract is represented in Fig. 4 as two air volumes separated by a pair of apertures. The buccal cavity is the volume of air in the mouth. From the buccal cavity, air flows through a pair of round or slit-like vocal sac apertures into an elastic vocal sac (Duellman and Trueb, 1994). The area of the vocal sac apertures can vary with pressure and muscle contractions (Martin and Gans, 1972; McAlister, 1959). The volume of the vocal sac changes during the call, with significant variation among species in the morphology and dynamics of this structure (Wells, 2007). For example, some sources suggest that the vocal sac may act like a balloon in which pressure is higher at low inflations (Dudley and Rand, 1991) while others show that pressure in the vocal sac increases only after some degree of inflation (Gridi-Papp, 2003).

The generally accepted qualitative model of anuran vocal production emphasizes the relationship between pressure within various volumes of the vocal system and the movement of elastic tissues (Gans, 1973; Martin, 1971; Martin and Gans, 1972; reviewed in Duellman and Trueb, 1994; Gerhardt and Huber, 2002; Wells, 2007). Several empirical studies have investigated how individual vocal system elements influence acoustic output. For example, artificial activation experiments on excised larynges in several taxa have demonstrated a relationship between airflow and linear and nonlinear frequency characteristics (Gridi-Papp, 2003; Martin, 1971; Suthers *et al.*, 2006). Within and among species, body size and/or vocal fold size is generally correlated with fundamental frequency (e.g., Gingras *et al.*, 2013; Martin, 1971; McClelland *et al.*, 1996). Martin (1971) used electrical stimulation to open the arytenoids of a toad; this increased tension on the vocal folds and their frequency of vibration. Gridi-Papp *et al.* (2006) showed that ablation of a fibrous mass associated with the túngara frog's vocal folds results in the loss of spectral structure in one of the call's components. Martin (1972) found that vocal sac muscles contract just after a toad's call, and Pauly *et al.* (2006) used

video analysis in túngara frogs to demonstrate that the vocal sac can act as an efficient mechanism for transferring air back to the lungs. Additionally, Martin (1972) and Gridi-Papp (2008) showed that bypassing the vocal sac of toads and treefrogs leads to changes in call amplitude and frequency, suggesting this structure's additional roles in coupling sounds to the environment and modulating the vibration of the vocal folds. A common conclusion is that the diversity of signals produced by anurans is both correlated with and constrained by variation in the anatomy and neuromuscular control of these vocal system elements (e.g., Boul and Ryan, 2004; Gans, 1973; McClelland *et al.*, 1998; McLean *et al.*, 2012; Ryan, 1988).

IV. BOND GRAPH MODEL OF THE INTEGRATED ANURAN VOCAL SYSTEM

In this section, we translate the description of the anuran vocal system from Sec. III into a bond graph that identifies both the physical relationships and causal interactions among its components (Fig. 5). Each vocal system component is represented in a generalized form that encompasses variation among anuran taxa in their anatomy and neuromuscular control. This model is thus a visual representation of the integrated anuran vocal system (*sensu* Borutzky, 2010) and a proposed framework for future bond graph modeling and simulation.

The model shown in Fig. 5 assumes bilateral symmetry. The lungs are a source of flow that provide energy to the system (Lu: element **Sf**). Compression of each lung reduces its volume over time and thus provides a volume flow rate to the rest of the system. At the **0-junction**, some of this flow is stored within the fluid capacitance of the lung (Lu: element **C**). The state of this fluid capacitance determines pressure in the lung, as indicated by the causal stroke at the **0-junction**. Flow that is not stored exits the lung.

Each bronchial passage is represented as a pipe. At the **1-junction**, some of the input from the adjoining lung is stored as pressure momentum within the bronchial passage (BP: element **I**). Volume flow rate through the bronchial passage is determined by this pressure momentum as indicated by the causal stroke at the **1-junction**. Some energy is dissipated because of friction caused by the walls of the pipe (BP: element **R**). From the bronchial passage, air enters the laryngeal apparatus as flow.

Some of the airflow into the posterior laryngeal chamber is stored in its fluid capacitance (LxP: element **C**); this determines pressure within the chamber. Some of the pressure in the posterior laryngeal chamber is transduced to a force that acts on each vocal fold at the transformer (VF: element **TF**). Each viscoelastic vocal fold is modeled here as a single mechanical mass-spring-damper system. Some of the force applied to the vocal fold is stored in the momentum of the tissue's mass (VF: element **I**). The velocity of the vocal fold depends on its momentum, as indicated by the causal stroke at the **1-junction**. Some of the force applied to the vocal fold is dissipated in its viscous properties (VF: element **R**). Likewise, some of the force applied to the vocal fold is stored in its elastic displacement (VF: element **C**). The displacement of the vocal fold supplies a restoring force to the system. The displacement of the vocal folds also determines the area of the aperture between them (VF: element **MR**). At the **1-junction**, this modulated resistor determines the volume flow rate between the vocal folds.

The anterior laryngeal chamber is modeled as another fluid capacitance (LxA: element **C**) and each arytenoid cartilage is modeled as a second mass-spring-damper system (AC: elements **I**, **C**, and **R**). The general relationships among these elements are as described above for the posterior laryngeal chamber and vocal folds. In this model, an additional force can potentially act on each arytenoid cartilage (AC: element **Se**); this represents active control of the arytenoid cartilages through a muscle force from outside the system. Flow exits the larynx through a variable aperture between the arytenoid cartilages (AC: element **MR**).

The buccal cavity is represented as a fourth fluid capacitance (BC: element **C**) that can store flow. Pressure in the buccal cavity depends on the state of this fluid capacitance, as indicated by the causal stroke at the **0-junction**. Flow between the buccal cavity and the vocal sac is determined by the area of the vocal sac aperture (VSA: element **R**) and by the pressure differential between the buccal cavity and the vocal sac. Modulation of the area of the vocal sac apertures is not included in the current model.

Pressure within the vocal sac depends on both its volume and the properties of its elastic tissues and muscles. To accommodate variability among species in the structure and dynamics of the vocal sac, the bond graph presented here models this structure as a combined compliance (Karnopp *et al.*, 2006,
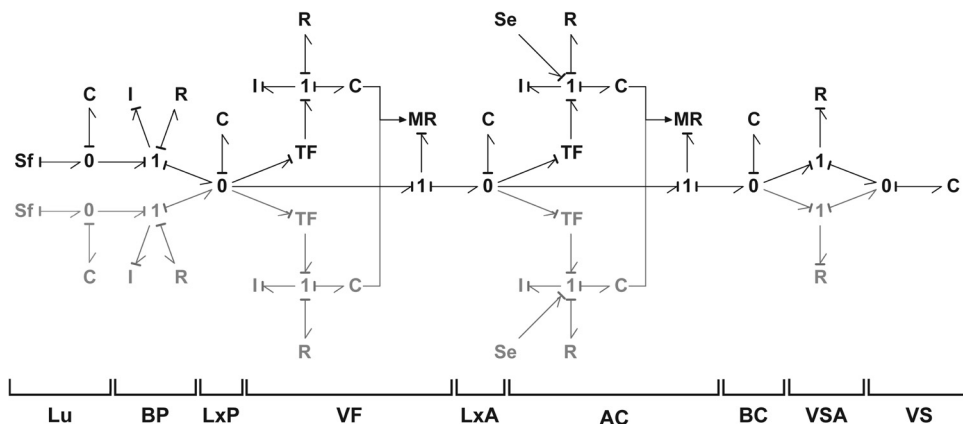

FIG. 5. Bond graph model of the anuran vocal system. All system components that are common among anuran taxa are included. Lu = lungs, BP = bronchial passages, LxP = posterior laryngeal chamber, VF = vocal folds, LxA = anterior laryngeal chamber, AC = arytenoid cartilages, BC = buccal cavity, VSA = vocal sac apertures, VS = vocal sac. Bilateral symmetry is indicated in gray.

p. 120) (VS: element **C**) that stores effort. The pressure in the vocal sac is determined by its combined compliance and the integrated flow that enters it, as indicated by the causal stroke at the **1-junction**.

In summary, this bond graph model of the anuran vocal system is one in which (1) a series of compliances represent pressures in different pneumatic components of the anuran vocal system, (2) mechanical mass-spring-damper systems are displaced when pressure is transformed to a force, and (3) pipes and apertures with variable areas gate airflow between system components. The causal relationships among vocal system components are in close alignment with qualitative models of the general mechanism of vocal production in anurans (e.g., Duellman and Trueb, 1994; Gans, 1973; Martin, 1971; Martin and Gans, 1972). It can thus be used as framework from which one can construct models based more explicitly on species-specific morphology or simulate system behavior using a set of constitutive relations and system parameters.

V. BOND GRAPH SIMULATION OF THE ANURAN SOUND SOURCE

One of the challenges in modeling air driven vocal production systems is that the sound source (e.g., the vocal folds in an anuran larynx) must exhibit sustained oscillations when coupled to air flow from the lungs (reviewed for tetrapods in Fitch and Hauser, 2003). These relatively high-frequency oscillations must be determined passively by the characteristics of the system's mechanical and pneumatic elements, and not by active control from the nervous system and muscles. This section describes a bond graph simulation of the anuran sound source that is capable of producing sustained oscillations with parameters that are realistic for a small frog.

A. Bond graph and equations

A bond graph model of the anuran sound source is shown in Fig. 6. Only half of the larynx is quantitatively

FIG. 6. Bond graph model of the anuran sound source. Only the top half of the bond graph is modeled, assuming bilateral symmetry as shown in gray. Indicated efforts (P = pressure, F = force) and flows (Q = volume flow rate, v = velocity) are discussed in the text.

modeled, assuming bilateral symmetry. The equations described below are valid for lumped element models of systems in which the size of any one component is small compared to the wavelength of sound produced (Fletcher, 1992); this is true in frogs, which produce low frequency signals for their body size (the túngara frog, for example, has a total body size of $\sim$30 mm and produces signals with frequencies less than 1000 Hz = 340 mm wavelength).

Following from the biological description in Sec. III and the integrated model in Sec. IV, this submodel begins with a source of flow (**Sf**) into the larynx from the lungs. The volume flow rate into the system from each lung is Q_{lu}.

At the first **0-junction**, some of the flow into the system is stored in the fluid capacitance of the posterior laryngeal chamber (**C**) at a rate equal to Q_{lxp}. The equation that determines the magnitude of Q_{lxp} is described later in this section because it depends on the behavior of other parts of the model. The displacement of air in the posterior laryngeal chamber is the integral of flow over time:

$$X_{lxp} = \int^t Q_{lxp}dt. \tag{1}$$

The conjugate output of the fluid capacitance is then the pressure in the posterior laryngeal chamber (as indicated by the causal stroke at the **0-junction**). At any given time this is

$$P_{lxp} = \frac{X_{lxp}}{C_{lxp}}, \tag{2}$$

where C_{lxp} is the compliance (compressibility) of the volume of air in the posterior laryngeal chamber. Compliance is determined by the standard equation

$$C_{lxp} = \frac{V_{lxp}}{\rho c^2}, \tag{3}$$

where V_{lxp} is the volume of the chamber, ρ is the density of air, and c is the speed of sound in air (Fletcher, 1992; Karnopp et al., 2006). Because the posterior laryngeal chamber is bounded by inflexible cartilage, we assume that its volume does not change.

At the transformer (**TF**), pressure in the posterior laryngeal chamber is transformed into a force that displaces each vocal fold from its initial resting position at the median of the larynx according to the relationship

$$F_{vf} = P_{lxp} * A_{vf}, \tag{4}$$

where A_{vf}, the transform ratio, is the effective area of the vocal fold against which air presses.

Each vocal fold is modeled as a viscoelastic mass-spring-damper system (**I**, **C**, and **R** elements, respectively). At the **1-junction**, the force applied to the vocal fold is partitioned among its elements. Part of this force is applied to its mass (**I**). The momentum of the vocal fold is the integral of force applied to its mass over time:

$$p_{vf} = \int^t F_{vfI}dt. \tag{5}$$

The conjugate output of this **I** element is then the velocity of the vocal fold, which at any given time is

$$v_{vf} = \frac{p_{vf}}{m_{vf}}, \tag{6}$$

where m_{vf} is mass of the vocal fold.

The velocity of the vocal fold influences several other aspects of the system, as indicated by the causal strokes at this **1-junction**. First, the displacement of each vocal fold is indicated by the state of its flow-storing spring (**C**). At any given time this equals the time-integrated velocity of the vocal fold:

$$X_{vf} = \int^{t} v_{vf} dt. \tag{7}$$

By Hooke's law, a displaced spring provides a restoring force proportional to its displacement and compliance (inverse of stiffness). As an initial simplification, each vocal fold is modeled as a linear spring and its restoring force is thus

$$F_{vfC} = \frac{X_{vf}}{C_{vf}}, \tag{8}$$

where C_{vf} is the compliance of the vocal folds in their range of free movement. If the two vocal folds collide at the median of the larynx, however, further displacement is restricted and impact oscillations may result. This can be modeled by increasing or adding spring forces at the point of collision (Ishizaka and Flanagan, 1972; Story and Titze, 1995). In this model, when the vocal fold reaches the median of the larynx, the restoring force supplied by the vocal fold changes to

$$F_{vfC} = \frac{X_{vf}}{C_{vf}} + \frac{X_{vf}}{C_{vf2}}, \tag{9}$$

where C_{vf2} is the decreased compliance of the vocal folds when they are at or beyond the median of the larynx.

Some of the force applied to the vocal folds is also dissipated by the viscous properties of the vocal fold tissue (**R**). The force dissipated from the system is

$$F_{vfR} = b_{vf} v_{vf}, \tag{10}$$

where b_{vf}, the damping coefficient of the vocal folds, is determined by the standard equation

$$b_{vf} = 2\zeta_{vf} \sqrt{\frac{m_{vf}}{C_{vf}}}, \tag{11}$$

in which ζ_{vf} is the damping ratio (Karnopp *et al.*, 2006). Note that the damping coefficient may change when the vocal folds collide at the median of the larynx (e.g., Ishizaka and Flanagan, 1972; Story and Titze, 1995); in this case, a modulated resistor with an input signal coming from the vocal fold compliance (**MR**) could be used instead. The current simulation was not sensitive to such a change.

Putting all of this together, the force against the mass of the vocal folds [for Eq. (5)] is

$$F_{vfI} = F_{vf} - F_{vfC} - F_{vfR}. \tag{12}$$

A third aspect of the system that is influenced by the velocity of the vocal folds is the volume flow rate at the transformer:

$$Q_{vf} = v_{vf} A_{vf}. \tag{13}$$

This is the conjugate output of the pressure in the posterior laryngeal chamber that is applied to the vocal folds

The final element of the bond graph in Fig. 6 models flow between the vocal folds as a function of their displacement (**MR**). This is modeled as an elliptical aperture with variable area. Because the vocal folds are attached to the arytenoids (Duellman and Trueb, 1994), one axis of the ellipse is fixed by the radius of the larynx (r_{lx}); the other axis of the ellipse depends on the displacement of the vocal folds. As the vocal folds move apart, the area of the aperture through which flow exits the posterior laryngeal chamber thus increases linearly with the magnitude of their displacement. In this model of the anuran sound source, there is no supra-laryngeal vocal tract. The pressure downstream of the vocal folds is simply modeled as a reference atmospheric pressure, **Se** = 0, and all pressures within the model are thus defined as deviations from atmospheric pressure. The rate of flow through this variable vocal fold aperture is determined by a nonlinear equation for flow through an orifice (e.g., Karnopp *et al.*, 2006, p. 117; Ishizaka and Flanagan, 1972; Riede *et al.*, 2011)

$$Q_{vfa} = C_d A_{vfa} \sqrt{\frac{2|P_{vfa}|}{\rho}} \mathrm{sgn} P_{vfa}, \tag{14}$$

where C_d is the discharge coefficient for flow through an aperture, A_{vfa} is the area of the aperture, P_{vfa} is the pressure difference between the posterior laryngeal chamber and the external environment (i.e., the input pressure to the modulated resistor, since $P_{lxp} - P_{atm} - P_{vfa} = 0$), $\mathrm{sgn} P_{vfa}$ is the sign of the pressure difference between the posterior laryngeal chamber and the supra-laryngeal environment, and ρ is the density of air.

One can now determine how much flow is stored in the fluid capacitance of the posterior laryngeal chamber. Because flows sum to zero at a 0-junction, the volume flow rate to the fluid capacitance is

$$Q_{lxp} = Q_{lung} - Q_{vf} - Q_{vfa}. \tag{15}$$

In summary, this model provides a means to quantify a generally accepted qualitative description of sound production by anurans (Gans, 1973; Martin, 1971; Martin and Gans, 1972). As in Martin's (1971) description, there are three integrators in this model. Pressure in the posterior laryngeal chamber is transduced to a force that influences the momentum of the vocal folds [Eq. (5)]. The momentum of the vocal folds, along with their mass, determines their velocity and thus the magnitude of their displacement [Eq. (7)]. This displacement determines the area of the vocal fold aperture, and thus modulates the amount of air flow through

it. This in turn influences the pressure in the posterior laryngeal chamber [Eq. (1)]. The constitutive equations described above further show how morphological system parameters such as laryngeal volume and vocal fold mass/tension can influence these integrators and cycles of vocal fold displacement and air flow between them.

B. Model parameters and simulation

Table III lists the parameters and constants needed to evaluate the equations above. The authors are unaware of any anuran species for which this complete set of parameters has been systematically measured. Most parameter values were therefore estimated from the currently available literature for a frog of the size of a túngara frog, *Physalaemus pustulosus* (~30 mm snout-vent length; see Fig. 3 for a call of this species) (Boul and Ryan, 2004; Dudley and Rand, 1991; McClelland *et al.*, 1996). An estimate for the damping ratio of the vocal folds is currently unavailable for anurans and was thus drawn from literature on other vertebrates (e.g., Riede *et al.*, 2011; Story and Tietze, 1995). Vocal fold compliance is variable in anurans (see Sec. III).

The software program 20-Sim (Controllab Products, B.V.) was used to perform simulations. The model was run for 0.7 s (about twice the duration of a *P. pustulosus* call; Fig. 3) using the program's variable time-step Backward Differentiation Formula as the integration method with absolute and relative tolerances of 1.0×10^{-15}. Model output variables included pressure within the posterior laryngeal chamber, displacement of the vocal folds, and volume flow rate of air through the vocal fold aperture as a function of time.

The primary indicator of the model's success was its ability to sustain oscillations in vocal fold displacement and air flow through the vocal fold aperture. A second indicator of the model's success was a frequency of oscillation that matches the fundamental frequency of advertisement calls produced by frogs. Fast Fourier transform (FFT) analysis was used to determine the oscillation frequency of vocal fold

TABLE III. Model parameters and constants for simulation of the anuran vocal folds.

	Parameter or Constant	Value
Q_{lu}	Flow rate from one lung	3×10^{-6} m^3/s [a]
V_{lxp}	Posterior laryngeal chamber volume (half)	6×10^{-8} m^3 [b]
r_{lx}	Larynx radius	3×10^{-3} m [b]
A_{vf}	Vocal fold effective area	2×10^{-6} m^2 [b]
m_{vf}	Vocal fold mass	3×10^{-7} kg [c]
C_{vf}	Vocal fold compliance	0.2 m/N [d]
C_{vf2}	Vocal fold compliance at the median of larynx	1×10^{-5} m/N [d]
ζ_{vf}	Vocal fold damping ratio	0.1 [d]
ρ	Density of air	1.21 kg/m^3 [e]
c	Speed of sound in air	343 m/s [e]
Cd	Discharge coefficient through orifice	0.62 [e]

Estimated from:
[a] Dudley and Rand (1991);
[b] Boul and Ryan (2004);
[c] McClelland *et al.* (1996);
[d] not available for anurans, see text;
[e] Karnopp *et al.* (2006).

displacement and volume flow rate through the vocal fold aperture.

To test the sensitivity of the model to its input parameter values, additional simulations varied individual system parameters between 25% and 250% of the values listed in Table III. Sensitivity data are reported for variation in four parameters that have been shown to have biological relevance (see Sec. III): flow rate from the lung, posterior laryngeal chamber volume, vocal fold mass, and vocal fold compliance. For each simulation, model output variables included maximum pressure in the posterior laryngeal chamber, maximum vocal fold displacement, and the fundamental frequency of vocal fold oscillations. Parameter values at which the model failed to show oscillations were also recorded.

C. Simulation results

A simulated bond graph model of the anuran sound source with parameters that are realistic for a small frog produces sustained oscillations in both vocal fold displacement and the rate of air flow between them (Fig. 7). At the beginning of the simulation, the vocal folds are at the median of the larynx. As air flows in from the lungs, pressure builds in the posterior laryngeal chamber [Fig. 7(A)], causing
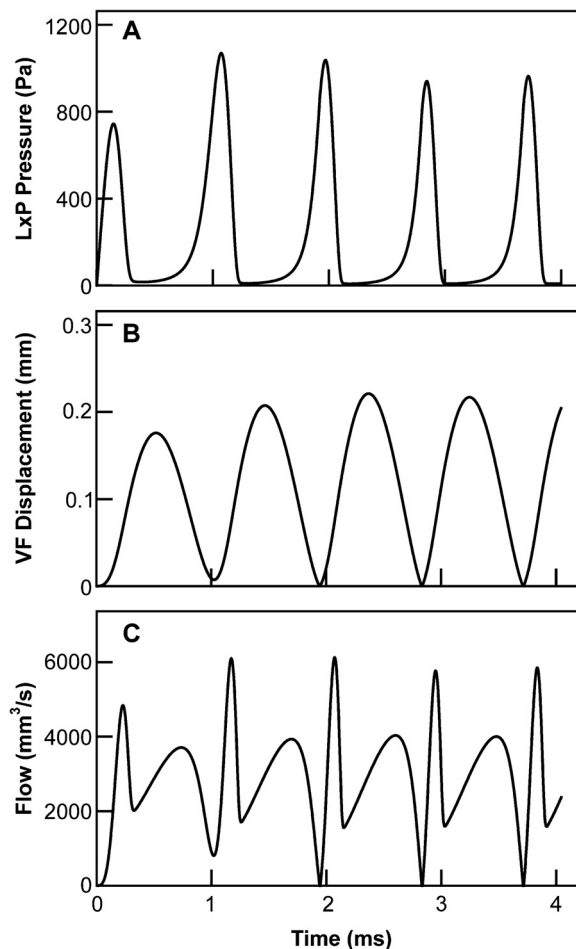

FIG. 7. Output for the first 4 ms of vocal fold model simulation. Pressure in the posterior laryngeal chamber (A), displacement of the vocal folds from the median of the larynx (B), and rate of flow through the vocal fold aperture (C).

Kime *et al.*: Bond graphs of anuran vocal systems

movement of the vocal folds away from the median of the larynx with a lag determined by their inertial mass [Fig. 7(B)]. Air begins to flow through the vocal fold aperture as the vocal folds are displaced [Fig. 7(C)]. When the sum of flow through the vocal fold aperture and the conjugate flow to the force on the vocal folds is greater than the flow into the posterior laryngeal chamber from the lungs [see Eq. (15)], the pressure differential in the larynx begins to decrease [Fig. 7(A)].

Although the momentum of the vocal folds causes them to continue moving apart for some time after pressure decreases, they eventually reverse direction and return to the median of the larynx because the restoring force of the vocal folds exceeds the force due to pressure in the posterior larynx [Fig. 7(B)]. In this model, the vocal folds can experience an impact force at the median of the larynx and make a sudden reversal in direction [Fig. 7(B)]. Pressure builds again in the time period during which the vocal folds are minimally displaced [Fig. 7(A)], and sustained oscillations in pressure and vocal fold displacement thus persist for the remainder of the simulation.

The rate of air flow between the vocal folds depends on both the area of the vocal fold aperture and the square root of the difference between pressure in the posterior laryngeal chamber and pressure downstream of the vocal folds [Eq. (14)]. Oscillations in flow therefore track oscillations in pressure and vocal fold displacement [Fig. 7(C), Fig. 8]. Volume flow rate between the vocal folds increases as pressure builds and the vocal folds move apart. It continues to increase even as pressure decreases as long as the rate at which the area of the vocal fold aperture increases due to momentum is larger than the rate at which the square root of pressure decreases (Fig. 8, arrow). A peak in flow through the vocal folds occurs when the vocal folds are opening and there is still some pressure differential in the larynx (Fig. 8, higher peak). Flow rate then decreases as pressure continues to drop and displacement of the vocal folds slows. A second peak in flow occurs when the vocal folds are closing and pressure is increasing (Fig. 8, lower peak). Flow again decreases as the vocal folds close.

When the model is simulated with the parameters listed in Table III, the vocal folds oscillate at a fundamental frequency of approximately 1100 Hz with visible harmonics caused by deviation from a simple sinusoid when the vocal folds collide at the median of the larynx [Fig. 9(A)]. Volume flow rate through the vocal fold aperture oscillates at a fundamental frequency of approximately1100 Hz with harmonics that reflect the nonsinusoidal nature of the oscillations [Fig. 9(B)].

Sustained oscillations persist across a wide range of parameter values but are not inevitable. They are not present when the volume flow rate from each lung is low ($<25\%$ of the value in Table III), the volume of the posterior laryngeal chamber is small ($<50\%$ of the value in Table III), or the vocal folds have little mass ($<50\%$ of the value in Table III). In all three of these situations, the vocal folds move apart but do not sustain oscillations as flow proceeds between them. Sustained oscillations also fail when vocal fold compliance is very high ($>200\%$ of the value in Table III).

Within the range of parameter values in which the model produces sustained oscillations, maximum pressure in the posterior laryngeal chamber increases when volume flow rate from the lungs increases or when the volume of the posterior laryngeal chamber decreases [Fig. 10(A)]. The maximum displacement of the vocal folds increases when volume flow rate from the lungs increases or when vocal fold compliance increases [Fig. 10(B)]. The fundamental frequency of vocal fold vibration increases with decreasing vocal fold mass or compliance; these two variables have nearly identical effects [Fig. 10(C)].

D. Discussion

The bond graph model of the anuran sound source described here behaves in a manner identical to Martin's (1971) qualitative model of sound production in the anuran larynx. Activation pressure in the posterior laryngeal
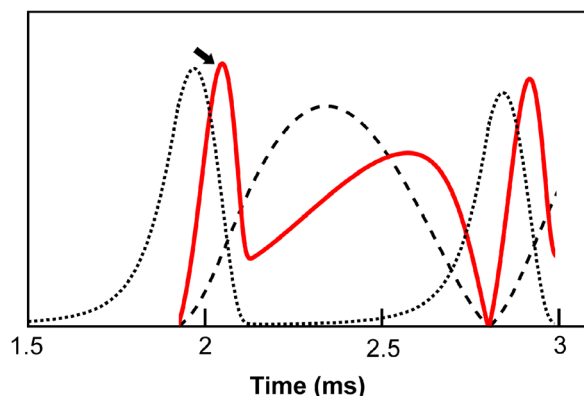

FIG. 8. (Color online) Rate of flow through the vocal folds (solid line) as a function of pressure in the posterior laryngeal chamber (dotted line) and vocal fold displacement (dashed line). Superimposed from model output presented in Fig. 7.
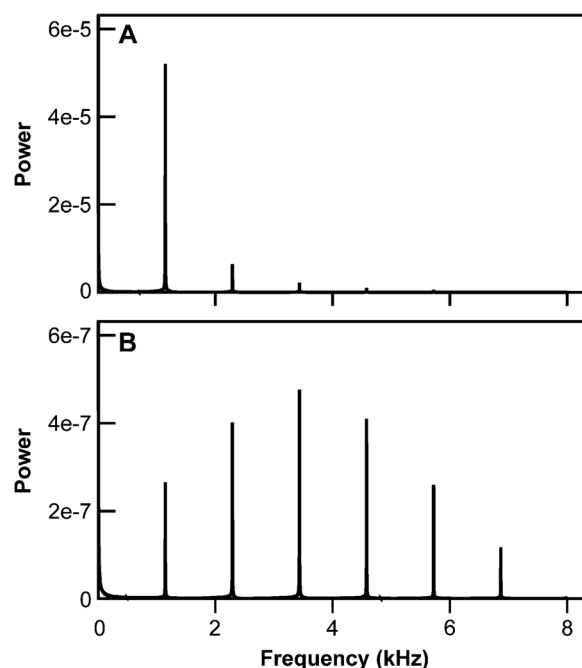

FIG. 9. Frequency of sustained oscillations in the vocal fold model simulation. FFT of vocal fold vibration (A) and volume flow through the larynx (B).
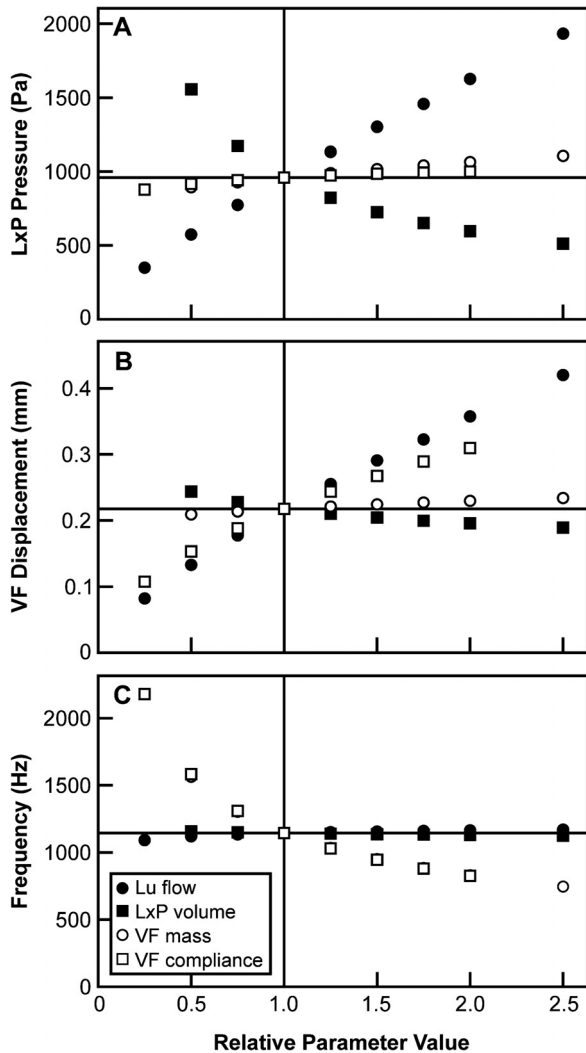
FIG. 10. Sensitivity of model output to changes in flow from the lungs, posterior laryngeal chamber volume, vocal fold mass, and vocal fold compliance. Maximum pressure in the posterior laryngeal chamber (A), maximum vocal fold displacement (B), and fundamental frequency of vocal fold oscillation (C). Reference lines indicate model output at parameter values listed in Table III.

chamber forces the vocal folds apart. The inertial mass of the vocal folds causes them to continue moving while pressure decreases as air flows out of the posterior larynx. Energy stored in the elasticity of the vocal folds causes them to close, and pressure again increases in the posterior laryngeal chamber. In the current bond graph model, as in Martin's description, lags in pressure within the laryngeal chamber and in the movement of the vocal folds are critically important to the ability of the model to sustain oscillations. For example, a posterior laryngeal chamber with low volume (where pressure changes rapidly) and vocal folds with low mass (which move rapidly) do not allow sustained oscillations. The importance of lags within the vocal system are also implicated in sustained oscillations of human vocal folds (e.g., Titze, 1988).

The influence of specific parameter values on the output of the model are also consistent with empirical studies of anuran vocal systems. First, the simulation presented here produces output with a fundamental frequency of approximately 1100 Hz; this is within the range of call frequencies produced by many anurans (e.g., Elliott *et al*., 2009; Ibañez *et al*., 1999). In the model, two determinants of oscillation frequency are the mass and compliance (tension) of the vocal folds. Vocal folds with large mass produce low frequency oscillations, and vocal folds with small compliance (high tension) produce high frequency oscillations. Several studies have suggested that these two anatomical parameters influence call frequency in anurans (e.g., Drewry *et al*., 1982; Gans, 1973; Gingras, 2013; Martin, 1971; Ryan and Drewes, 1990; Wells, 2007).

Second, flow from the lungs influences oscillations of the vocal folds. Low flow from the lungs does not allow sustained oscillations; this is consistent with artificial activation experiments in frogs and toads that show a threshold pressure for sound production (Gridi-Papp, 2003; Martin and Gans, 1972; Suthers *et al*., 2006). On the other hand, in these experiments, increasing flow and pressure upstream of the vocal folds increased the frequency of sound produced by the larynx (Gridi-Papp, 2003; Martin, 1971; Suthers *et al*., 2006). Suthers *et al*. (2006) also produced signal nonlinearities and chaos characteristic of the torrent frog's call by varying pressure in an excised larynx. This is not the case in the model presented here. Altering the rate of air flow from the lungs causes only small changes in frequency; these are due to changes in the collision of the vocal folds at their medial boundary. One addition to the current model that would introduce a relationship between air flow and frequency is a hardening spring in which compliance decreases with vocal fold displacement (unpublished data). The rapid displacement of the vocal folds that results from increased air flow would then be reversed more quickly by their restoring force, thus increasing frequency.

The presence of harmonics in anuran advertisement calls varies among species, and in some cases within species (e.g., Feng *et al*., 2002). In the current model of a simple sound source, harmonics result primarily from nonsinusoidal oscillations in volume flow rate between the vocal folds (Elemans *et al*., 2008). Flow is nonsinusoidal because it depends on both pressure differential and vocal fold displacement (e.g., Fig. 8) and also because of collision of the vocal folds at their medial boundary. It has been suggested that harmonics in frog calls result from nonsinusoidal vibration of the vocal folds (e.g., Gerhardt and Huber, 2002; Feng *et al*., 2002; Martin, 1971). The role of vocal fold impacts on harmonic signals has been discussed for humans and birds (e.g., Tao *et al*., 2006; Zaccarelli *et al*., 2006) and alluded to in frogs (Martin, 1971).

The simplified bond graph model described here can be viewed as one from which to begin further study of the anuran vocal system. There are three possibilities. First, a complete set of parameter values from one or more species of anuran is necessary to fully evaluate the model. Second, morphological data from individual species may suggest ways to increase the complexity of the model in species-specific ways, such as including nonlinear compliances or the fibrous masses found in some species. A third direction for future study is to add other components of the vocal system described in Secs. III and IV to determine how interactions among the lungs, larynx, and vocal tract influence sustained oscillations of the

vocal folds and the spectral and temporal characteristics of sound produced by an integrated system.

VI. CONCLUSIONS

This paper shows how bond graphs can be used to model air-driven vocal production systems such as those found in birds, mammals, and anurans (frogs and toads). There is general consensus regarding the mechanism of sound production in anurans, which emphasizes the relationship between pressure within various volumes of the vocal system and the movement of elastic tissues (Gans 1973; Martin, 1971; Martin and Gans, 1972; see also Duellman and Trueb, 1994; Gerhardt and Huber, 2002; Wells 2007). As described in Sec. V, simulation of a simple bond graph model of the anuran sound source validates this longstanding model by producing sustained oscillations in vocal fold displacement and air flow through the larynx with input parameters that are realistic for a small frog. In this model, as in previous empirical studies (e.g., Gingras, 2013; Gridi-Papp, 2003; Martin, 1971; McClelland et al., 1996; Suthers et al., 2006), the presence and frequency of sustained oscillations depend on pressure in the posterior larynx and the size and tension of the vocal folds. Further exploration of this and similar models should provide further insights into the biomechanics of vocal production in anurans.

The sound source is only one component of the vocal system, and bond graphs can also be used to investigate how it interacts with the lungs and supra-laryngeal vocal tract. Previous authors have suggested that the sound produced within the anuran larynx may be influenced by pressure in the lungs, buccal cavity, and vocal sac; it may also be modulated by the oscillatory behavior of other vocal system components such as the arytenoid cartilages (Dudley and Rand, 1991; Gans, 1973; Feng et al., 2002; Martin, 1971, 1972; Martin and Gans, 1972). The bond graph of the integrated frog vocal system presented in Sec. IV provides a gateway for future work on the relationship among vocal system components, both in interpreting previous results (such as why puncturing the vocal sac changes call frequency, e.g., Martin, 1972) and in generating predictions for future experimental studies. This model can also provide information about which anatomical parameters are important to understanding sound production in a given species.

There has been considerable interest in the evolution of the anuran communication system because of its role in sexual selection and speciation (Gerhardt and Huber, 2002; Ryan, 2001). For male vocal production, much of the focus has been on the evolution of acoustic signals; numerous studies have examined interspecific call variation in a phylogenetic context to elucidate patterns of call evolution (e.g., Castellano et al., 2002; Cocroft and Ryan, 1995; Gergus et al., 2010; Ryan and Rand, 1995). There has been less focus on the evolution of underlying mechanisms; fewer studies have investigated the relationship between variation in advertisement calls and variation in the morphology of the male vocal system (e.g., Boul and Ryan, 2004; McClelland et al., 1996; Ryan, 1986). Furthermore, interpreting such studies is difficult because the vocal system is a complex

adaptation that relies upon the functional integration of several traits. The modeling approach illustrated here will allow researchers to investigate the relationship between the evolution of morphology and acoustic signals, especially how it might be influenced or constrained by the functional congruence of separate morphological traits.

Aroyan, J. L., McDonald, M. A., Webb, S. C., Hildebrand, J. A., Clark, D., Laitman, J. T., and Reidenberg, J. S. (2000). "Acoustic models of sound production and propagation," *Hearing by Whales and Dolphins*, edited by W. W. L. Au, A. N. Popper, and R. R. Fay (Springer, New York), pp. 409–469.

Borutzky, W. (2009). "Bond graph modeling and simulation of multidisciplinary systems–An introduction," Simul. Model. Pract. Theory 17, 3–21.

Borutzky, W. (2010). *Bond Graph Methodology: Development and Analysis of Multidisciplinary Dynamic System Models* (Springer-Verlag, London), 662 pp.

Boul, K. E., and Ryan, M. J. (2004). "Population variation of complex advertisement calls in *Physalaemus petersi* and comparative laryngeal morphology," Copeia 2004, 624–631.

Breedveld, P. C. (2004). "Port-based modeling of mechatronic systems," Math. Comput. Simul. 66, 99–127.

Busch-Vishniac, I. J., and Paynter, H. M. (1989). "Bond graph models of sound and vibration systems," J. Acoust. Soc. Am. 85, 1750–1758.

Castellano, S., Cuatto, B., Rinella, R., Rosso, A., and Giacoma, C. (2002). "The advertisement call of the European treefrogs (*Hyla arborea*): A multilevel study of variation," Ethology 108, 75–89.

Cocroft, R. B., and Ryan, M. J. (1995). "Patterns of advertisement call evolution in toads and chorus frogs," Anim. Behav. 49, 283–303.

de Boer, B. (2009). "Acoustic analysis of primate air sacs and their effect on vocalization," J. Acoust. Soc. Am. 126, 3329–3343.

Drewry, G. E., Heyer, W. R., and Rand, A. S. (1982). "A functional analysis of the complex call of the frog *Physalaemus pustulosus*," Copeia 1982, 636–645.

Dudley, R., and Rand, A. S. (1991). "Sound production and vocal sac inflation in the túngara frog, *Physalaemus pustulosus* (Leptodactylidae)," Copeia 1991, 460–470.

Duellman, W. E., and Trueb, L. (1994). *Biology of Amphibians* (Johns Hopkins University Press, Baltimore), Chapter 4, pp. 87–107.

Elemans, C. P. H., Heeck, K., and Muller, M. (2008). "Spectrogram analysis of animal sound production," Bioacoustics 18, 183–212.

Elemans, C. P. H., Larsen, O. N., Hoffmann, M. R., and van Leeuwen, J. L. (2003). "Quantitative modelling of the biomechanics of the avian syrinx," Anim. Biol. 53, 183–193.

Elliott, L., Gerhardt, H. C., and Davidson, C. (2009). *The Frogs and Toads of North America: A Comprehensive Guide to their Identification, Behavior, and Calls* (Houghton Mifflin, Boston, MA), 344 pp.

Feng, A. S., Narins, P. M., and Xu, C. H. (2002). "Vocal acrobatics in a Chinese frog, *Amolops tormotus*," Naturwiss. 89, 352–356.

Fitch, W. T., and Hauser, M. D. (2003). "Unpacking 'honesty': Vertebrate vocal production and the evolution of acoustic signals," in *Acoustic Communication*, edited by A. M. Simmons, R. R. Fay, and A. N. Popper (Springer, New York), pp. 65–137.

Fletcher, N. H. (1988). "Bird song−A quantitative acoustic model," J. Theor. Biol. 135, 455–481.

Fletcher, N. H. (1992). *Acoustic Systems in Biology* (Oxford University Press, New York), 352 pp.

Fletcher, N. H., and Thwaites, S. (1979). "Physical models for the analysis of acoustical systems in biology," Q. Rev. Biophys. 12, 25–65.

Gans, C. (**1973**). "Sound production in the Salientia: Mechanism and evolution of the emitter," Am. Zool. **13**, 1179–1194.

Gergus, E. W. A., Sullivan, B. K., and Malmos, K. B. (**2010**). "Call variation in the *Bufo microscaphus* complex: Implications for species boundaries and the evolution of mate recognition," Ethology **103**, 979–989.

Gerhardt, H. C., and Huber, F. (**2002**). *Acoustic Communication in Insects and Anurans* (University of Chicago Press, Chicago), 542 pp.

Gingras, B., Boeckle, M., Herbst, C. T., and Fitch, W. T. (**2013**). "Call acoustics reflect body size across four clades of anurans," J. Zool. **289**, 143–150.

Gridi-Papp, M. (**2003**). "Mechanism, behavior, and evolution of calling in four North American treefrogs," Ph.D. dissertation, University of Texas at Austin.

Gridi-Papp, M. (**2008**). "The structure of vocal sounds produced with the mouth closed or with the mouth open in treefrogs," J. Acoust. Soc. Am. **123**, 2895–2902.

Gridi-Papp, M., Rand, A. S., and Ryan, M. J. (**2006**). "Complex call production in the túngara frog," Nature **441**, 38.

Ibañez, R., Rand, A. S., and Jaramillo, C. A. (**1999**). *The Amphibians of Barro Colorado Nature Monument, Soberania Natural Park and Adjacent Areas* (Editorial Mizrachi y Pujol, Panama). 187 pp.

Ishizaka, K., and Flanagan, J. L. (**1972**). "Synthesis of voiced sounds from a two-mass model of the vocal cords," Bell Syst. Tech. J. **51**, 1233–1268.

Karnopp, D. C., Margolis, D. L., and Rosenberg, R. C. (**2006**). *System Dynamics: Modeling and Simulation of Mechatronic Systems* (Wiley, New York), 576 pp.

Martin, W. F. (**1971**). "Mechanics of sound production in toads of the genus *Bufo*: Passive elements," J. Exp. Zool. **176**, 273–293.

Martin, W. F. (**1972**). "Evolution of vocalization in the genus *Bufo*," in *Evolution in the Genus Bufo*, edited by W. F. Blair (University of Texas Press, Austin), pp. 279–309.

Martin, W. F., and Gans, C. (**1972**). "Muscular control of the vocal tract during release signaling in the toad *Bufo valliceps*," J. Morphol. **137**, 1–27.

McAlister, W. H. (**1959**). "The vocal structures and method of call production in the genus *Scaphiopus holbrook*," Tex. J. Sci. **11**, 60–77.

McClelland, B. E., Wilczynski, W., and Ryan, M. J. (**1996**). "Correlations between call characteristics and morphology in male cricket frogs (*Acris crepitans*)," J. Exp. Biol. **199**, 1907–1919.

McClelland, B. E., Wilczynski, W., and Ryan, M. J. (**1998**). "Intraspecific variation in laryngeal and ear morphology in male cricket frogs (*Acris crepitans*)," Biol. J. Linn. Soc. **63**, 51–67.

McLean, M. J., Bishop, P. J., and Nakagawa, S. (**2012**). "Assessing the patterns of evolution in anuran vocal sexual signals," Evol. Biol., DOI: 10.1007/s11692-012-9197-0.

Pauly, G. B., Bernal, X. E., Rand, A. S., and Ryan, M. J. (**2006**). "The vocal sac increases call rate in the túngara frog *Physalaemus pustulosus*," Physiol. Biochem. Zool. **79**, 708–719.

Riede, T., Tokuda, I. T., and Farmer, C. G. (**2011**). "Subglottal pressure and fundamental frequency control in contact calls of juvenile *Alligator mississippiensis*," J. Exp. Biol. **214**, 3082–3095.

Ryan, M. J. (**1986**). "Factors influencing the evolution of acoustic communication: Biological constraints," Brain Behav. Evol. **28**, 70–82.

Ryan, M. J. (**1988**). "Constraints and patterns in the evolution of anuran acoustic communication," in *The Evolution of the Amphibian Auditory System*, edited by B. Fritzsch, M. J. Ryan, W. Wilczynski, T. E. Hetherington, and W. Walkowiak (Wiley, New York), pp. 637–677.

Ryan, M. J., Ed. (**2001**). *Anuran Communication* (Smithsonian Institution Press, Washington, DC), 252 pp.

Ryan, M. J., and Drewes, R. C. (**1990**). "Vocal morphology of the *Physalaemus pustulosus* species group (Leptodactylidae): Morphological response to sexual selection for complex calls," Biol. J. Linn. Soc. **40**, 37–52.

Ryan, M. J., and Rand, A. S. (**1995**). "Female responses to ancestral advertisement calls in túngara frogs," Science **269**, 390–392.

Schmidt, R. S. (**1965**). "Larynx control and call production in frogs," Copeia **1965**, 143–147.

Story, B. H. (**2002**). "An overview of the physiology, physics and modeling of the sound source for vowels," Acoust. Sci. Technol. **23**, 195–206.

Story, B. H., and Titze, I. R. (**1995**). "Voice simulation with a body-cover model of the vocal folds," J. Acoust. Soc. Am. **97**, 1249–1260.

Suthers, R. A., Narins, P. M., Lin, W., Schnitzler, H., Denzinger, A., Xu, C., and Feng, A. S. (**2006**). "Voices of the dead: Complex nonlinear vocal signals from the larynx of an ultrasonic frog," J. Exp. Biol. **209**, 4984–4993.

Tao, C., Jiang, J. J., and Zhang, Y. (**2006**). "Simulation of vocal fold impact pressures with a self-oscillating finite-element model," J. Acoust. Soc. Am **119**, 3987–3994.

Titze, I. R. (**1988**). "The physics of small-amplitude oscillation of the vocal folds," J. Acoust. Soc. Am. **83**, 1536–1552.

Titze, I. R. (**2000**). *Principles of Voice Production* (National Center for Voice and Speech, Iowa City), 407 pp.

Wells, K. D. (**2007**). *The Ecology and Behavior of Amphibians* (University of Chicago Press, Chicago), Chap. 7, pp. 268–337.

Zaccarelli, R., Elemans, C. P., Fitch, W., and Herzel, H. (**2006**). "Modelling bird songs: voice onset, overtones and registers," Acta Acoust. **92**, 741–748.